

# Nonlinear thermal and electronic optical properties of graphene in N-methylpyrrolidone at 800 nm with femtosecond laser pulses

Cite as: J. Appl. Phys. **124**, 033104 (2018); <https://doi.org/10.1063/1.5025781>

Submitted: 13 February 2018 . Accepted: 02 July 2018 . Published Online: 20 July 2018

R. Weigand, M. Sánchez-Balmaseda , S. M. Afanador-Delgado , and H. J. Salavagione 



View Online



Export Citation



CrossMark

## ARTICLES YOU MAY BE INTERESTED IN

[A cavity ring-down spectrometer for study of biomedical radiocarbon-labeled samples](#)

Journal of Applied Physics **124**, 033101 (2018); <https://doi.org/10.1063/1.5041015>

[Linear-field plasma jet arrays excited by high-voltage alternating current and nanosecond pulses](#)

Journal of Applied Physics **124**, 033301 (2018); <https://doi.org/10.1063/1.5036704>

[Ultraviolet optical excitation of near infrared emission of Yb-doped crystalline aluminum oxynitride thin films](#)

Journal of Applied Physics **124**, 033102 (2018); <https://doi.org/10.1063/1.5040340>

## Ultra High Performance SDD Detectors



See all our XRF Solutions

# Nonlinear thermal and electronic optical properties of graphene in N-methylpyrrolidone at 800 nm with femtosecond laser pulses

R. Weigand,<sup>1,a)</sup> M. Sánchez-Balmaseda,<sup>2</sup> S. M. Afanador-Delgado,<sup>3</sup> and H. J. Salavagione<sup>4</sup>

<sup>1</sup>Departamento de Óptica, Facultad de Ciencias Físicas, Universidad Complutense de Madrid, E-28040 Madrid, Spain

<sup>2</sup>Departamento de Estructura de la Materia, Física Térmica y Electrónica, Facultad de Informática, Universidad Complutense de Madrid, E-28040 Madrid, Spain

<sup>3</sup>Departamento de Ciencias Exactas y Tecnológicas, Universidad de Guadalajara (CULAGOS), Enrique Díaz de León 1144, Paseos de La Montaña, 47460 Lagos de Moreno, Jalisco, Mexico

<sup>4</sup>Departamento de Física de Polímeros, Elastómeros y Aplicaciones Energéticas, Instituto de Ciencia y Tecnología de Polímeros, CSIC, C/ Juan de la Cierva 3, E-28006 Madrid, Spain

(Received 13 February 2018; accepted 2 July 2018; published online 20 July 2018)

Graphene is a useful saturable absorber in a variety of lasers working in mode-locking or Q-switch regimes. The optical performance of chemically synthesized graphene is still not completely characterized. In this study, the saturable absorption and the nonlinear refractive index of graphene flakes in N-methylpyrrolidone, in both liquid and solid phases, have been studied at 800 nm with the z-scan technique using femtosecond laser pulses. The results obtained using a Ti:sapphire laser oscillator in the mode-locking regime (6 fs, 78 MHz) or in the continuous wave shows that the optical properties of graphene have a thermal origin, while at the lower repetition rate and higher energy and intensity of a Ti:sapphire amplifier (95 fs, 1 kHz), it shows the electronic Kerr effect. Solid samples with very high optical densities, equivalent to 60 layers of graphene grown by chemical vapor deposition (CVD), can be fabricated. They show a higher saturation intensity ( $I_s \approx 100 \text{ GW cm}^{-2}$ ) than CVD-grown ( $74 \text{ MW cm}^{-2}$ ) or epitaxially grown ( $4 \text{ GW cm}^{-2}$ ) graphene and intensity-dependent changes in transmission from 25% to 43%. This change in transmission in multilayer solid samples points to a good performance as a saturable absorber in laser cavities. *Published by AIP Publishing.*

<https://doi.org/10.1063/1.5025781>

## I. INTRODUCTION

Graphene, either physically or chemically synthesized, is a relatively new material which has attracted much attention because of its distinctive physical properties, including the optical ones. Graphene related materials, such as graphene oxide, also show similar interesting optical properties.

In the last years, much work has been done in the optical characterization of graphene and other graphene related materials in different spectral zones and temporal ranges.

Representative works include the study with the z-scan technique<sup>1</sup> of the nonlinear refractive and absorptive optical properties of graphene grown by chemical vapor deposition (CVD) or epitaxially, reporting values of  $n_2 = 10^{-7} \text{ cm}^2 \text{ W}^{-1}$ ,<sup>2</sup> or more recently,  $n_2 = -1.1 \times 10^{-9} \text{ cm}^2 \text{ W}^{-1}$ ,<sup>3</sup> for the nonlinear refractive index of monolayer graphene, and  $I_s = 74 \text{ MW cm}^{-2}$ ,<sup>2</sup> or  $4 \text{ GW cm}^{-2}$  (Ref. 4) for the saturation intensity. These results indicate that the optical properties of graphene are sensitive to various parameters, such as doping.<sup>3</sup> The optical properties of suspensions of graphene, graphene oxide, and other derivatives have also been studied.<sup>5–12</sup>

N-methylpyrrolidone (NMP) is an excellent solvent for graphene in the sense that very high concentrations of graphene can be reached by sonication of graphite and that the stability of the suspensions is high.<sup>13,14</sup> While graphene has been

optically characterized in a variety solvents,<sup>15</sup> there are only few works in NMP<sup>16–18</sup> using infrared lasers with fs and ns pulse duration or at 532 nm with ns pulse durations, and mostly on saturable absorption (SA) and optical limiting. Given the high concentrations that can be reached in NMP, optically dense films can be prepared by deposition of some drops on a glass substrate and subsequent solvent evaporation or desiccation. This has the advantage that graphene films can be fabricated in an easy way with a high optical density, equivalent to a multilayer CVD (Chemical Vapor Deposition)-grown graphene, which is much more expensive and time consuming to fabricate. This work aims to explore the nonlinear optical characteristics of liquid suspensions of graphene in NMP and in solid form, obtained by desiccation on glass substrates, at 800 nm using femtosecond laser pulses.

## II. EXPERIMENTAL SECTION

### A. Laser sources

We used two laser sources. One was a Ti:sapphire oscillator operating in the mode-locking (ML) regime at 78 MHz with an average power of 100 mW and pulse duration of 6 fs,<sup>19</sup> or operating in a continuous wave (cw) with an average power of 120 mW. To perform temporally resolved measurements, a light chopper was employed (see Sec. IID). The other laser was a Ti:sapphire amplifier with a pulse duration of 95 fs and a repetition rate of 1 kHz, with pulse energies up to 1 mJ. Both lasers were linearly polarized.

<sup>a)</sup>Electronic mail: weigand@fis.ucm.es

## B. Preparation of graphene in NMP

The liquid exfoliation of graphite<sup>13</sup> or expanded graphite<sup>20</sup> is widely used to prepare a dispersion of graphene in an organic solvent like NMP. A graphene dispersion in NMP was prepared by ultrasonic treatment of expanded graphite (Angstrom Materials, N002-PDR) for 20 min, by using a UP400S ultrasonic processor (Hielscher). Then, the heavier parts of the sample (graphitic species) were left to precipitate overnight, and the supernatant was collected. It is known that the higher the sonication time, the higher the concentration of dispersed particles and the lower the flake size.<sup>21</sup> In this case, the lateral size of the as-produced flakes ranges from sub-micron up to a few micrometers. The concentration of the dispersion was determined gravimetrically by passing it through a pre-weighted fluoropore membrane (0.2  $\mu\text{m}$  pore size), obtaining a value of ca. 0.8 mg ml<sup>-1</sup>.

## C. Preparation of samples

The optical study was done in liquid suspensions and solid samples. The liquid suspensions were obtained by diluting the stock suspension. For the measurements with the oscillator, we started by adding a 2  $\mu\text{l}$  drop with a micropipette to a 300  $\mu\text{l}$  fused silica cuvette with a 1 mm optical path length, filled with NMP. The divergence of the beam when focused on the sample (see Sec. II D) was very strong to be able to collect the whole beam within the detector's area, even at short distances, which on the other side can damage the detector. Hence, this suspension was further diluted with NMP up to  $5.3 \times 10^{-4}$  mg ml<sup>-1</sup>, until the observed divergence was small enough to perform the open aperture (OA) measurements (see Sec. II D) with the detector positioned out of the translation stage of the sample. For the measurements with the amplifier, 8  $\mu\text{l}$  of the stock suspension was added to a fused silica cuvette with a 1 mm optical path length, filled with 300 microl of NMP.

The solid samples were made by dropping several drops of the stock suspension (sample S1/1) or a 1/4 diluted suspension (sample S1/4) onto a standard microscope cover glass whose lateral edges had been delimited with a scotch tape, forming a square of approximately  $8 \times 8$  mm<sup>2</sup>. The pure solvent or the suspension was left to dry at room temperature for more than one day. This procedure resulted in much more homogeneous samples than those done with heat treatment in an oven at 60–80 °C. We obtained samples with a reasonable uniform distribution of the material [Figs. 1(a) and 1(b)]. Figures 1(c) and 1(d) show the atomic force microscope (AFM) images of samples S1/1 and S1/4. We can observe that the flakes have micron-sized areas, with a quite homogeneous distribution and that they pile-up in a disordered manner up to a total thickness of around hundreds of nanometers, namely, approximately 400 nm for S1/1, 800 nm for S1/4, and 670 nm for NMP, as deduced using the software for data treatment of the AFM. These thicknesses can be also seen in the black and white height scale in Fig. 1. To identify the composition of the solid sample, Raman spectra were taken (Fig. 2). The most important features in the Raman spectra are the G band appearing around 1585 cm<sup>-1</sup>, an intense disorder-induced D band at 1348 cm<sup>-1</sup>,

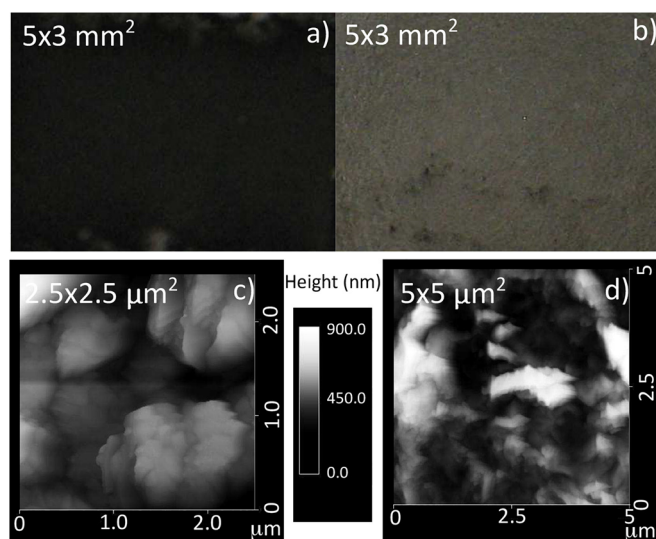


FIG. 1. Picture of a solid sample done by evaporation of some drops of (a) the stock solution 1/1 (sample S1/1) or (b) diluted to 1/4 (sample S1/4). AFM images of samples (c) S1/1 and (d) S1/4.

the second order 2D band at around 2690 cm<sup>-1</sup>, and the D+G band at 2933 cm<sup>-1</sup>, indicating the presence of multi-layer graphene.<sup>22</sup> Raman spectra collected at different points in the samples were reproducible, indicating a certain degree of uniformity. In addition, Raman spectra before and after irradiation are almost identical, with a very similar  $I_D/I_G$  ratio. Since the areas illuminated by the Raman laser and the Ti:sapphire are similar, this reveals no degradation due to the laser measurements.<sup>23</sup>

Further characterization on the flakes dimensions and thicknesses was conducted by transmission electron microscopy (TEM), using a JEOL 3000F electron microscope operated at 300 kV for a 1/4 diluted suspension. Figure 3(a) shows a large area on the grid, where more homogeneous (A1) and more wrinkled flakes (A2) can be observed. Figure 3(b) shows a higher resolution image where several flakes can be seen piled-up in four different zones (Z1–Z4). Z1 shows the smallest number of flakes, and Z2–Z4 seem to be adding a layer at a time. Figure 3(c) shows a large resolution image in a zone similar to Z4 along with its electron diffraction pattern. A similar diffraction pattern was obtained in zone A2. The apparent amorphous structure observed in Figs. 3(b) and 3(c) along with the electron diffraction pattern evidences that the sheet is graphene. In the case of having

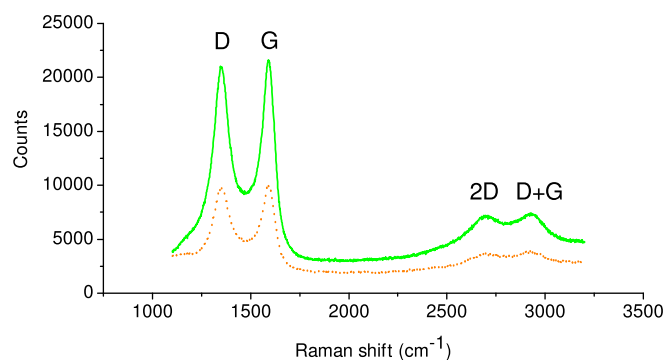


FIG. 2. Raman spectrum of the solid samples S1/1 (solid line) and S1/4 (dotted line).

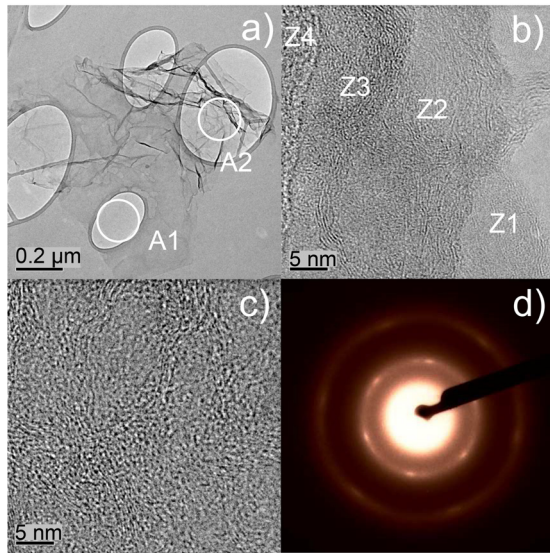


FIG. 3. (a) Low resolution TEM image showing large graphene flakes, (b) high resolution TEM image showing a superposition of layers, (c) high resolution TEM image in a multilayer zone such as Z4, and (d) the electron diffraction pattern in a multilayer zone.

graphite-like sheets, the electron diffraction pattern would show a hexagonal distribution of perfectly well shaped reflections, and the corresponding high-resolution image would show the lattice constants. Instead, we observed a ring-like electron diffraction pattern, indicating a disordered stack of several graphene layers. The results are in agreement with the Raman spectra, and we can assume that the samples consist of disordered piled-up graphene layers, which cannot be considered graphite-like structures.

From now on we will call NMP as a sample of pure NMP (either liquid or desiccated), and G as a sample of graphene in NMP (either a liquid suspension or a desiccated suspension). To distinguish between the liquid and solid phases, we will use prefixes L and S, respectively. To distinguish between measurements done with the oscillator or the amplifier, we use cw for the oscillator in the continuous wave, ML for the oscillator in mode-locking, and A for the amplifier. Thus, a measurement done in liquid NMP with the oscillator in mode-locking will be identified as NMP-L-ML, in the cw mode as NMP-L-cw, a measurement in a solid sample of the evaporated suspension of graphene in NMP with the amplifier as G-S-A, etc.

Each sample was characterized by its linear transmission with the Ti:sapphire laser oscillator operating in cw. For the liquid samples, we obtained  $T_{\text{NMP}} = 95\%$  for pure NMP and  $T_{\text{NMPG}} = 94\%$  for the suspension of graphene in NMP, at the low concentrations used in the oscillator experiments, and  $T_{\text{NMPG}} = 63\%$  at the higher concentration used in the experiments with the amplifier. For the solid samples, we obtained  $T_{\text{NMP}} = 93\%$  for evaporated NMP,  $T_{\text{NMPG}} = 25\%$  for S1/1, and  $T_{\text{NMPG}} = 65\%$  for S1/4. For a more complete characterization, ultraviolet (UV)-visible (Vis)-near infrared (NIR) transmission spectra (Fig. 4) were measured using a UV-Vis-NIR spectrometer (Shimadzu UV-3100) equipped with an integrating sphere, so that only changes in transmittance due to absorption were detected. In Fig. 4(a), the transmission of liquid NMP (95%) and graphene suspensions

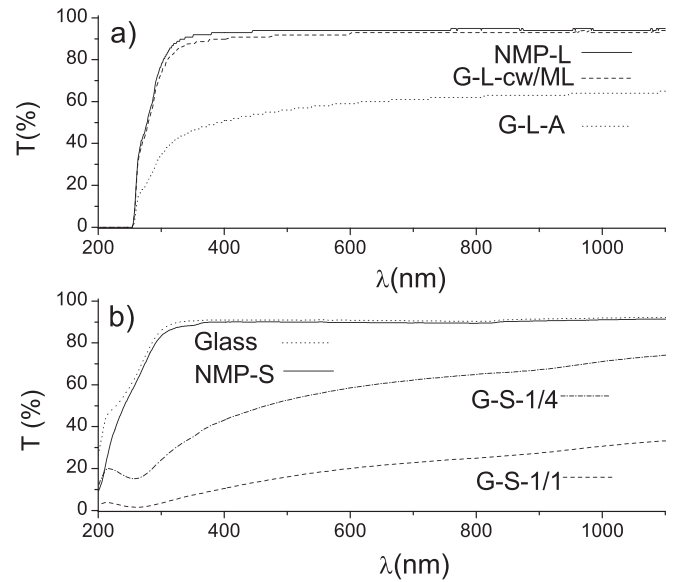


FIG. 4. Transmittance of the different samples.

(94% for the oscillator in cw or ML and 63% for the amplifier) at 800 nm can be seen. The curves are very flat, as expected, since NMP absorbs in the deep UV, and graphene is a zero band-gap material. The decay below 300 nm is due to the absorption of the cuvette, and the sample G-L-A seems to have a larger absorption in the UV around 400 nm than in the Vis-NIR zone. In Fig. 4(b), both the glass substrate and desiccated NMP display a flat transmission but the desiccated suspensions of graphene in NMP have an increasing absorption towards the UV. This is in agreement with previous reports,<sup>24</sup> where an increased UV absorption of CVD-grown graphene with the number of layers is observed. In our case, the UV absorption is also larger for the sample with the higher number of layers (G-S-1/1) and in the most concentrated suspension (G-L-A).

Using the values of the transmittance  $T$  at 800 nm, we can estimate the equivalent number of CVD-grown graphene layers necessary to have the same  $T$ . A single layer of graphene has 2.3% absorbance (hence, a transmittance  $T = 1 - 0.023 = 0.977$ ) and a thickness  $d = 3.35 \times 10^{-10}$  m. According to Lambert-Beer's law, the transmitted intensity is  $I_1 = I_0 e^{-\alpha_1 d}$ , where  $I_0$  is the incident intensity,  $I_1$  the transmitted intensity, and  $\alpha_1$  is the absorption coefficient of a single graphene layer. Hence,  $I_1/I_0 = 0.977 = e^{-\alpha_1 d}$ . A multilayer sample with  $m$  layers will transmit  $I_m = I_0 (e^{-\alpha_1 d})^m$ . Hence,  $I_m/I_0 = (e^{-\alpha_1 d})^m = 0.977^m = T_m$ , where  $T_m$  is the transmittance of the  $m$ -layers sample. Therefore,  $m$  can be estimated as  $m = \ln(T_m)/\ln(0.977)$ . In our samples, we have  $m = 59.5$  for  $T = 25\%$  and  $m = 18.5$  for  $T = 65\%$ , which are much higher than the thicknesses obtained with bottom-up approaches like CVD or epitaxial growing. These values are in agreement with the Raman spectra in Fig. 2 and the AFM (Fig. 1) and TEM (Fig. 3) measurements, where we concluded that we have piled-up multi-layer graphene.

#### D. The z-scan technique

The nonlinear optical properties were measured using the z-scan technique in open aperture (OA) and closed

aperture (CA) configurations (Fig. 3). This technique is most widely used to characterize the nonlinear absorptive properties and nonlinear refractive index of materials because of its sensitivity and, in principle, rather easy implementation.<sup>1</sup>

OA measurements give information about nonlinear absorption. For a medium with transmittance  $T$  and saturable absorption, the intensity dependent nonlinear absorption coefficient  $\alpha(I)$  at the intensity  $I$  is given by

$$\alpha(I) = \frac{\alpha_0}{1 + I/I_s}, \quad (1)$$

where  $\alpha_0$  is the linear absorption coefficient and  $I_s$  is the saturation intensity.<sup>25</sup> The transmitted intensity for a sample of length  $L$  will be given by

$$I_t = Ie^{-\alpha(I)L} \quad (2)$$

or equivalently

$$\alpha(I) = -\frac{\ln(I_t/I)}{L}. \quad (3)$$

Thus, one can measure  $I_t$  with an OA z-scan, in which at each point  $z$  the intensity  $I$  can be calculated by Gaussian beam propagation, and fit the results obtained with Eq. (2) or (3) to  $\alpha(I)$  from Eq. (1) to deduce the saturation intensity  $I_s$ . Or, alternatively, one can position the sample at the focus of the focusing system and measure the transmitted intensity  $I_t$  for different input intensities  $I$ , thus obtaining the saturation curve of Eq. (3), which can be then fit using Eq. (1) to obtain again the saturation intensity  $I_s$ . In order to collect the whole beam, we have included a lens in our set-up (Fig. 5) before the detector module (or iris+detector module). This guarantees that appropriate detection of nonlinear absorption is done and that no fraction of the beam is lost due to, for example, scattering losses.

On the other hand, CA measurements inform about changes in the refractive index. For a medium with the pure Kerr effect, the refractive index will be given by  $n = n_0 + n_2I$ , where  $n_0$  is the linear refractive index and  $n_2$  is the nonlinear Kerr index, which causes an on-axis phase-change  $\Delta\Phi$  in the beam given by

$$\Delta\Phi = n_2I_0kL_{eff}, \quad (4)$$

where  $k$  is the modulus of the wave vector,  $I_0$  is the on-axis intensity at  $z = 0$ , and  $L_{eff}$  is the effective length given by  $L_{eff} = (1 - e^{-\alpha_0L})/\alpha_0$ . The normalized transmittance through a closed aperture is given by<sup>2</sup>

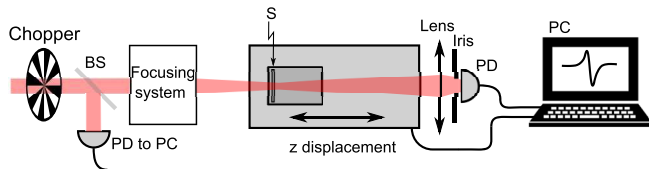


FIG. 5. Schematic diagram of the z-scan technique for the open aperture (iris removed) and closed aperture configurations. BS, beam splitter; PD, photodetector; PC, computer; S, sample. The chopper is used only in time resolved measurements.

$$T = 1 + \frac{4\Delta\Phi x}{(1+x^2)(9+x^2)}, \quad (5)$$

where  $x = z/z_R$ ,  $z$  is the sample position with respect to the focus and  $z_R$  is the Rayleigh range. The fit of the experimental z-scan curves for the CA configuration using Eq. (5) leads to the determination of the sign and magnitude of  $n_2$ . For the pure electronic Kerr effect,  $n_2$  is proportional to the third order susceptibility  $\chi^{(3)}$ . For a sample with the Kerr effect plus saturable absorption (SA) or two-photon absorption (TPA), the absorptive effects would superpose to the closed aperture measurement. Hence, in practice, closed aperture measurements are always divided by the open aperture measurements before fitting.<sup>1</sup>

When using high-repetition lasers, thermal effects may appear which create a temperature gradient across the laser spot, and the local changes in the refractive index affect the divergence of the beam. In this case, the transmittance through the closed aperture follows other laws. For example, using an aberrant thermal lens model, the transmittance can be described as follows:<sup>26,27</sup>

$$T = \left[ 1 + \frac{\Delta\Phi}{2} \tan^{-1} \left( \frac{2x}{1+x^2} \right) \right]^2 \quad (6)$$

or more accurately as<sup>28</sup>

$$T = \left[ 1 + \frac{\Delta\Phi}{2} \tan^{-1} \left( \frac{2x}{3+x^2} \right) \right]^2. \quad (7)$$

$\Delta\Phi$  also adopts the form in Eq. (4), but  $n_2$  is proportional to the change in the refractive index with temperature  $dn/dT$ .<sup>29</sup> Unlike the purely optical Kerr effect which, due to its electronic origin, can be considered instantaneous, thermal effects are slow and it takes some time until the material system has evolved to a stationary situation. Thus, attempts have been done to follow the temporal evolution of the thermal effect. For that purpose, a chopper is used to switch the light on and off, and the temporal evolution of the transmittance can be recorded using an oscilloscope coupled to a photodetector. In some cases, the transit from purely electronic behaviour to thermal behaviour has been observed.<sup>30</sup> A distinctive feature of z-scan graphs is the peak-valley (p-v) separation. In the case of the purely Kerr effect, the p-v separation amounts  $1.7 z_R$ , while in the case of thermal effect the p-v separation can be larger (for instance around  $3.4 z_R$  in Ref. 31). This separation can also be used to identify whether the thermal effects are dominating.

The laser beam radii were measured just before the focusing element at  $1/e^2$  of the peak intensity using the razor blade technique.<sup>32</sup> We obtained  $480 \mu\text{m}$  in the cw regime and  $420 \mu\text{m}$  in the mode-locking regime for the oscillator and  $1.4 \text{ mm}$  for the amplifier. When using the oscillator, the beam was focused using a parabolic silver mirror with a focal length of  $5 \text{ cm}$ . A parabolic mirror was used instead of a lens because of the short duration of the laser pulse, since a lens would temporally lengthen the pulse by GVD (Group Velocity Dispersion). When using the amplifier, a lens with a focal length of  $10 \text{ cm}$  was employed, which is adequate for

the longer pulse of the amplifier, with less spectral content. With these parameters, the beam waist at the focus  $w_0$  and the Rayleigh range  $z_R$  were calculated using standard Gaussian beam propagation (oscillator in mode-locking:  $w_0 = 30 \mu\text{m}$ ,  $z_R = 3.6 \text{ mm}$ , oscillator in cw:  $w_0 = 26 \mu\text{m}$ ,  $z_R = 2.8 \text{ mm}$ , and amplifier:  $w_0 = 18.2 \mu\text{m}$ ,  $z_R = 1.3 \text{ mm}$ ). The samples thicknesses were thus within the Rayleigh range in all configurations, as required by the technique (1 mm path length for the cuvette and  $\sim 150 \mu\text{m}$  of the substrate plus hundreds of nanometers of graphene for the solid samples).

The samples were placed on a movable stage with several centimeters path length, and the intensity in the closed or open aperture configuration was registered with a large area ( $1 \times 1 \text{ cm}^2$ ) photodiode. For the CA configuration, an iris was placed before the detector to set the aperture linear transmittance at  $S = 0.5$ . This setting is a good compromise between having large signals and averaging possible beam non-uniformities. A second photodiode was used as reference to compensate for possible intensity fluctuations in the laser. The whole system was computer controlled, and the intensity at each point on the  $z$  axis was averaged over 200 points. This further hindered possible intensity fluctuations of the laser to contaminate the measurements. The solid samples were measured in different positions, and the results were averaged to avoid misleading results from possible inhomogeneities.

In order to evaluate the importance of the thermal effect, in our studies, we also placed a chopper in the beam path of the oscillator (Fig. 5) and was operated at 200 Hz. This repetition rate along with a multiblade wheel resulted in a time resolution of microseconds. The photodetector was connected to a digital oscilloscope (1 MHz bandwidth) working in average mode, so that for each  $z$ , 64 oscilloscope traces were averaged and then saved. The whole system (motor + detection system) was totally automated using the software LabVIEW.

### III. RESULTS AND DISCUSSION

#### A. Results with the oscillator

From the data of the average power, repetition rate, and beam size given in Secs. II A and II D, we can estimate the intensity at focus in cw and mode-locking regimes.

##### 1. Liquid suspensions

The open aperture measurements showed neither saturable absorption (SA) nor two-photon absorption (TPA) under the conditions of this study. The results obtained in the closed aperture  $z$ -scan configurations for the liquid samples, in both cw and mode-locking regimes can be seen in Figs. 6(a) and 6(b) and show a negative effect, in both cw and ML regimes for liquid NMP and G (NMP-L-cw, G-L-cw, NMP-L-ML, and G-L-ML). The effect in pure liquid is much smaller than for the suspensions of graphene. Moreover, there is no significant difference between the results obtained for cw and ML. This hints for the fact that the effect is mainly from the thermal origin.

We tried to identify the presence of a possible electronic behavior at short times by using the set-up with the temporal

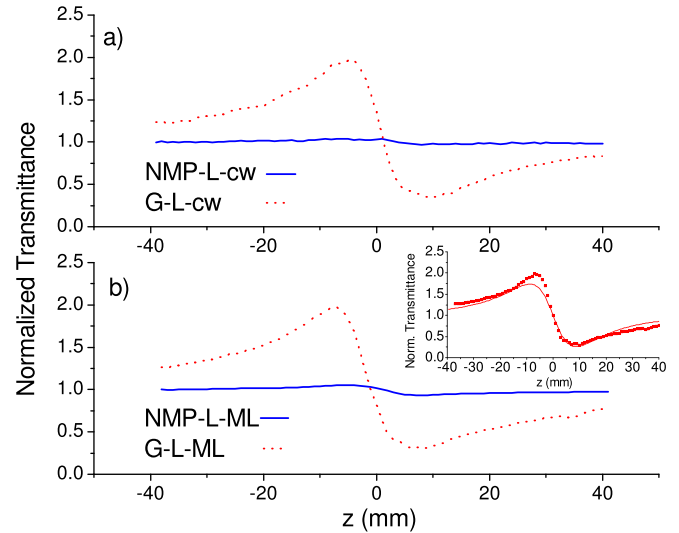


FIG. 6. CA measurements for liquid NMP and suspensions of graphene in NMP with the oscillator in (a) cw and (b) mode-locking regimes. Inset: The CA  $z$ -scan curve for G-L-ML and its fit using Eq. (7).

resolution. The result for the liquid suspension of graphene using the oscillator in the mode-locking regime is shown in Fig. 7. We can observe that the scan traces slowly evolve until its final value and that the sign of the traces is the same at all times. Moreover, the peak-valley distance is the same at short and long times and is larger than  $1.7 z_R$ . This indicates that even at short times, the thermal effect is already predominant versus a Kerr effect of electronic origin. Similar results were obtained for pure NMP. Hence, if we want to detect the Kerr effect, we have to study the system at much shorter times and lower repetition rates (see Sec. III B).

The value of the thermal  $n_2$  was calculated by fitting the CA curves obtained without the chopper using Eq. (7), which properly accounts for thermal effects. Since in the case of the oscillator in the ML regime we are handling with thermal effects,  $I$  was calculated using the average power of the pulse train (120 mW in cw and 100 mW in mode-locking) and not with the energy of the pulse. The inset in Fig. 6(b) shows, as an example, the fit of G-L-ML. The results can be seen in Table I and always show a negative value, as expected for

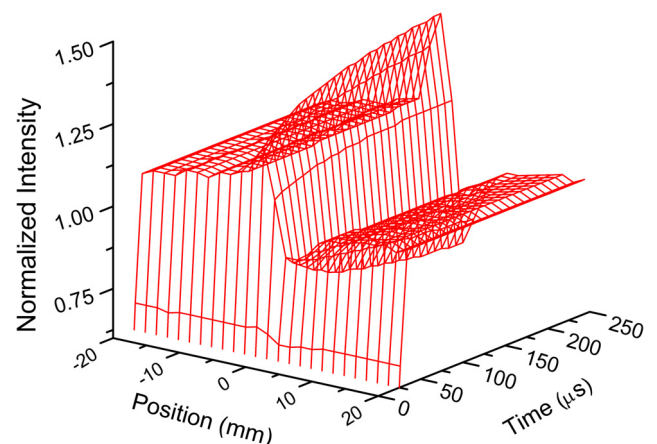


FIG. 7. Time resolved CA measurements for a suspension of graphene in NMP with the oscillator.

TABLE I. Summary of results obtained for the different samples with the oscillator in continuous wave (cw) and mode-locking (ML) regimes.

| Sample   | SA | $n_2$ sign | p-v/ $z_R$ | Thermal $n_2$ ( $\text{cm}^2\text{W}^{-1}$ ) |
|----------|----|------------|------------|--|
| NMP-L-cw | No | Negative   | 6          | $-1.5 \times 10^{-9}$                        |
| G-L-cw   | No | Negative   | 6          | $-4 \times 10^{-8}$                          |
| NMP-L-ML | No | Negative   | 4          | $-4 \times 10^{-9}$                          |
| G-L-ML   | No | Negative   | 4          | $-6 \times 10^{-8}$                          |
| NMP-S-cw | No | Positive   | 8.4        | $8 \times 10^{-6}$                           |
| G-S-cw   | No | Positive   | 8.4        | $1.5 \times 10^{-5}$                         |
| NMP-S-ML | No | Positive   | 3.2        | $6 \times 10^{-6}$                           |
| G-S-ML   | No | Positive   | 3.2        | $4 \times 10^{-5}$                           |

liquids.<sup>27</sup> The p-v distance divided by the corresponding  $z_R$  is also shown and in all cases is higher than 1.7, corroborating that we are in a thermal regime.

## 2. Solid samples

Unlike for liquid samples, the effect has a positive sign in both cw and ML regimes for the solid samples of NMP and sample S1/1 (NMP-S-cw, G-S-cw, NMP-S-ML, and G-S-ML) as shown in Fig. 8. In this case, the samples with graphene do not exhibit a larger effect than NMP alone, either in cw or ML regimes. Again, there are no significant differences between cw and ML regimes, indicating a thermal origin for the effect. Again, the measurements done with the temporal resolution could not differentiate between electronic and thermal effects. The thermal effect is already present at short times after the chopper blades turns on the light and could also be recognized by the peak-valley distance of the scan traces. By fitting the stationary traces obtained without the chopper in Fig. 8 (using 120 mW in cw and 100 mW in mode-locking), we obtain the values of  $n_2$  in Table I. In this case, the thermal  $n_2$  values are always positive, as is usual in glasses.<sup>27</sup>

For the solid sample, the transmission curve in different OA measurements remains constant, so we conclude that saturable absorption was not detectable, and no damage was done during the measurements either in the form of an ablation hole or a carbonization dot.

From the results described above, we observe that G samples have the same sign of the refractive index as its corresponding solvent, either in the liquid or solid state. This fact indicates that NMP strongly influences the effect on the G samples, both in the cw and in the high-repetition rate regimes.

## B. Results with the amplifier

The results obtained with the oscillator indicate that the thermal effect builds up at short times, so we used a lower rate Ti:sapphire amplifier operating at 1 kHz to measure the nonlinear refractive index due the Kerr-effect.

The intensities used can be deduced with the repetition rate, pulse duration, average power, and beam size at focus given in Secs. II A and II D. The values of these estimated intensities at focus will be given for every average power value used in the experiment.

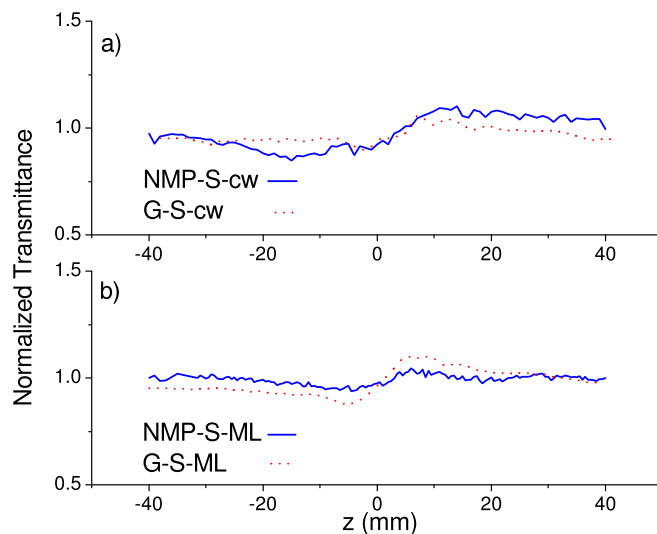


FIG. 8. CA measurements for desiccated NMP and desiccated suspensions of graphene in NMP with the oscillator in (a) cw and (b) mode-locking regimes.

## 1. Liquid suspensions

Figure 9(a) shows the results obtained with the z-scan in the open aperture regime for liquid NMP (NMP-L-A) and liquid suspensions of graphene in NMP (G-L-A) at  $400 \mu\text{W}$  ( $I = 4 \times 10^{11} \text{ W cm}^{-2}$ ). While the solvent NMP-L-A shows no absorption up to average power of  $500 \mu\text{W}$  ( $I = 5 \times 10^{11} \text{ W cm}^{-2}$ ), the graphene suspension G-L-A shows saturable

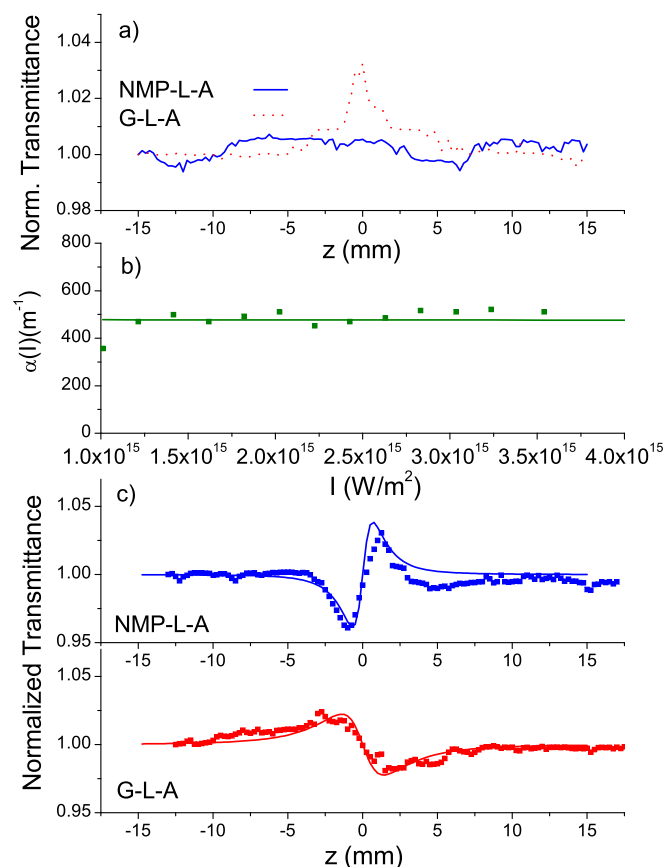


FIG. 9. (a) OA and (c) CA measurements for liquid NMP and graphene in NMP with the amplifier and their fits. (b) Saturation curve and fit.

TABLE II. Summary of results obtained for the different samples with the amplifier (A).

| Sample    | SA  | $I_s$ (W cm <sup>-2</sup> ) | $n_2$ sign | p-v/ $z_R$ | Kerr $n_2$ (cm <sup>2</sup> W <sup>-1</sup> ) |
|-----------|-----|-----------------------------|------------|------------|---|
| NMP-L-A   | No  | ...                         | Positive   | 1.6        | $7 \times 10^{-17}$                           |
| G-L-A     | Yes | $>10^{14}$                  | Negative   | 1.9        | $-7 \times 10^{-17}$                          |
| NMP-S-A   | No  | ...                         | Positive   | 2          | $6 \times 10^{-14}$                           |
| G-S-A 1/1 | Yes | $4 \times 10^{11}$          | Negative   | 1.8        | $-0.9 \times 10^{-13}$                        |
| G-S-A 1/4 | Yes | $7 \times 10^{11}$          | Negative   | 2          | $-1.6 \times 10^{-13}$                        |

absorption, as can be seen in Fig. 9(a). For powers larger than  $400 \mu\text{W}$  ( $I = 4 \times 10^{11} \text{ W cm}^{-2}$ ), supercontinuum due to phase modulation is generated, and we enter in another non-linear regime, so the rest of the measurements were done below this value. Figure 9(b) shows the saturation curve  $\alpha(I)$  for G-L-A obtained from the measurements using Eq. (3) and the fit using Eq. (1). The curve  $\alpha(I)$  is very flat, and the fit requires a very large value of the saturation intensity  $I_s > 10^{14} \text{ W cm}^{-2}$ .

Figure 9(c) shows the results obtained with the z-scan in the closed aperture regime for liquid NMP (NMP-L-A) and liquid suspensions of graphene in NMP (G-L-A) using the laser amplifier at an average power of  $350 \mu\text{W}$  ( $I = 3.5 \times 10^{11} \text{ W cm}^{-2}$ ), after dividing by the OA curves to obtain the purely refractive behavior. The solvent NMP shows a positive effect, opposite to the sign obtained when the oscillator was employed. This reveals the different origin of the refractive nonlinearity, which should be of the electronic origin with the amplifier. The graphene sample (G-L-A) has a negative Kerr effect, i.e., the opposite sign to NMP-L-A, as plotted in Fig. 9(c). In this case, the behavior in graphene is not dominated by the solvent. Also in both cases, the separation peak-valley amounts around  $1.7 z_R$ , indicating the absence of the thermal effect at the repetition rate of 1 kHz. The results obtained for  $I_s$ , Kerr  $n_2$  [fits using Eqs. (1) and (5), respectively], and p-v/ $z_R$  ratio are summarized in Table II.

## 2. Solid samples

Figure 10(a) shows the results obtained in the open aperture z-scan for the two samples of evaporated graphene in NMP (G-S-A S1/1 and S1/4) at  $500 \mu\text{W}$  ( $I = 5 \times 10^{11} \text{ W cm}^{-2}$ ). While no absorption changes were detected in NMP-S-A for average power up to  $500 \mu\text{W}$  ( $I = 5 \times 10^{11} \text{ W cm}^{-2}$ ), both G-S-A samples clearly show a strong saturated absorption. Sample S1/1 has a linear transmission  $T = 25\%$ ; hence, the peak at  $z = 0 \text{ mm}$ , which reaches a normalized transmission of 1.73 in Fig. 10(a), corresponds to a nonlinear transmittance of  $1.73 \times 0.25 = 0.43$  and the transmittance has almost doubled. For CVD-grown graphene, with a saturation intensity of  $I_s = 74 \text{ MW cm}^{-2}$ ,<sup>2</sup> one needs 30 layers to have a change in transmittance from 1 to 1.73, which are obviously difficult to grow by CVD. An increase in transmission  $\Delta T = 0.73$  in the estimated  $m = 59$  layers gives 1.24% absorption change per layer, far from the maximum 2.3% possible, and less than the reported change of 5.1% for 3 CVD-grown graphene layers.<sup>2</sup> For the solid sample, the transmission curve in the OA measurement in Fig.

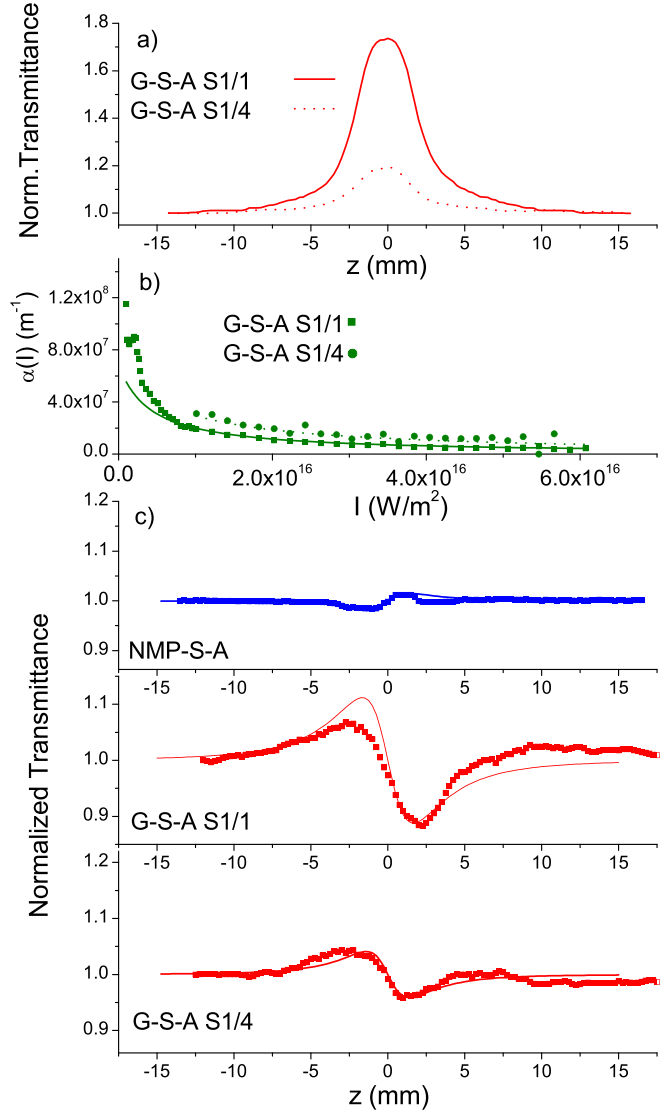


FIG. 10. (a) OA and (c) CA measurements for solid NMP and graphene in NMP (S1/1 and S1/4) with the amplifier and their fits. (b) Saturation curves and fit.

10(a) is symmetric, so we conclude that no damage was done during the measurements either in the form of an ablation hole or a carbonization dot. Note that the ablation of a single graphene layer would result in a change of 2.3% in the transmission value. No TPA was observed.

The saturation curves measured with the samples placed in focus are shown in Fig. 10(b). The saturation intensity  $I_s$  is deduced by fitting the saturation curves using Eq. (1). The results are shown in Table II and indicate higher saturation values than those obtained by other authors with CVD or epitaxial growing, but more similar to the results obtained by other authors in chemically produced graphene.<sup>15,17</sup>

Figure 10(c) shows the results obtained with the closed aperture z-scan for evaporated NMP (NMP-S-A) at  $650 \mu\text{W}$  ( $I = 6.5 \times 10^{11} \text{ W cm}^{-2}$ ) and the two samples of evaporated graphene in NMP (G-S-A S1/1 and S1/4) at  $150 \mu\text{W}$  ( $I = 1.5 \times 10^{11} \text{ W cm}^{-2}$ ) and  $600 \mu\text{W}$  ( $I = 6 \times 10^{11} \text{ W cm}^{-2}$ ), respectively, after dividing by the corresponding OA curves to have the pure Kerr behavior. Again, NMP-S-A shows a positive Kerr effect, as we obtained in the liquid state using

the amplifier. But both G-S-A samples show a negative Kerr-effect, as obtained in liquid suspensions with the amplifier. This corroborates again that the effect measured with the amplifier is an optical Kerr-effect of the electronic origin, while the change in the refractive index was of the thermal origin when using the oscillator, in which we obtained the positive thermal effect for the solid samples, and the behavior in graphene seemed to be influenced by the state of the solvent. Also, as in the case of liquid suspensions measured with the amplifier, the peak-valley separation amounts around  $1.7 z_R$ , indicating the absence or extremely low influence of the thermal effect at the repetition rate of 1 kHz.

The value of  $n_2$  was calculated by fitting the CA curves using Eq. (5), and we obtained smaller values than other authors for CVD grown graphene.<sup>2</sup> The results are summarized in Table II.

#### IV. CONCLUSION

We have studied the saturable absorption and the nonlinear refractive index of graphene in N-methylpyrrolidone at 800 nm, either in suspensions or in desiccated form, using two ultrafast laser sources, namely a Ti:sapphire oscillator and a Ti:sapphire amplifier. In the experiments with the oscillator, no saturable absorption was observed either in the liquid or solid form, due to the low pulse energy. The refractive index change is negative in the liquid form and positive in the solid form in both cw and ML and has the same sign as in the solvent. Since the measurements done with the oscillator in the cw regime gave similar results to those in the ML regime, the p-v separation amounts much more than  $1.7 z_R$ , we conclude that the effect in this set of measurements is of the thermal origin. This was corroborated by the measurements with the temporal resolution, in which a fast growth of the thermal effect during tens of  $\mu\text{s}$  was observed.

In experiments with the amplifier, no saturable absorption was observed for liquid or solid NMP, but for G, a strong SA in the solid form (weaker in the liquid form) has been measured. The saturation intensities  $I_s$  ( $\approx 4\text{--}7 \times 10^{11} \text{ W cm}^{-2}$ ) were higher than those obtained by other authors for CVD-grown graphene ( $74 \text{ MW cm}^{-2}$ )<sup>2</sup> or epitaxially grown graphene ( $4 \text{ GW cm}^{-2}$ )<sup>4</sup> but more similar than for chemically produced graphene ( $300 \text{ GW cm}^{-2}$ ,  $60 \text{ GW cm}^{-2}$ ).<sup>15,17</sup>

Strong bleaching has been observed, with changes in the normalized transmittances from 1 to 1.73, using the amplifier. The Kerr effect observed in solid samples of graphene with the amplifier was negative and smaller in absolute values than other data for monolayer CVD-grown graphene in the literature.<sup>3</sup> This is not surprising since discrepancies in the values of  $n_2$  have been previously encountered and attributed to doping by other authors.<sup>3</sup> The different sign of the z-scan traces obtained as compared to measurements done with the oscillator, as well as the peak-valley separation, supports the hypothesis that the change in the refractive index in this set of measurements done with the amplifier is indeed due to the Kerr effect of electronic origin.

The fact that no damage was observed during the measurements and that the solid samples are easily fabricated can be seen as an advantage for fabricating samples of high

optical density and strong bleaching capacity, and they can be used as a saturable absorber in laser cavities.

#### ACKNOWLEDGMENTS

We gratefully acknowledge the support from projects Santander-Complutense FIS2013-41709-P, MAT2013.47898-C2-2-R, and PCIN2016-021(M-ERA-NET2/0002/2016) from MINECO. Also, ICTS Centro Nacional de Microscopía Electrónica (Universidad Complutense de Madrid, Spain) for the AFM and TEM measurements.

<sup>1</sup>M. Sheik-Bahae, A. Said, T.-H. Wei, D. Hagan, and E. W. Van Stryland, "Sensitive measurement of optical nonlinearities using a single beam," *IEEE J. Quantum Electron.* **26**, 760–769 (1990).

<sup>2</sup>H. Zhang, S. Virally, Q. Bao, L. K. Ping, S. Massar, N. Godbout, and P. Kockaert, "Z-scan measurement of the nonlinear refractive index of graphene," *Opt. Lett.* **37**, 1856–1858 (2012).

<sup>3</sup>E. Dremetsika, B. Dlubak, S.-P. Gorza, C. Ciret, M.-B. Martin, S. Hofmann, P. Seneor, D. Dolfi, S. Massar, P. Emplit, and P. Kockaert, "Measuring the nonlinear refractive index of graphene using the optical Kerr effect method," *Opt. Lett.* **41**, 3281–3284 (2016).

<sup>4</sup>G. Xing, H. Guo, X. Zhang, T. C. Sum, and C. H. A. Huan, "The physics of ultrafast saturable absorption in graphene," *Opt. Express* **18**, 4564–4573 (2010).

<sup>5</sup>X.-L. Zhang, X. Zhao, Z.-B. Liu, Y.-S. Liu, Y.-S. Chen, and J.-G. Tian, "Enhanced nonlinear optical properties of graphene-oligothiophene hybrid material," *Opt. Express* **17**, 23959–23964 (2009).

<sup>6</sup>Y. Liu, J. Zhou, X. Zhang, Z. Liu, X. Wan, J. Tian, T. Wang, and Y. Chen, "Synthesis, characterization and optical limiting property of covalently oligothiophene-functionalized graphene material," *Carbon* **47**, 3113–3121 (2009).

<sup>7</sup>Z.-B. Liu, Y.-F. Xu, X.-Y. Zhang, X.-L. Zhang, Y.-S. Chen, and J.-G. Tian, "Porphyrin and fullerene covalently functionalized graphene hybrid materials with large nonlinear optical properties," *J. Phys. Chem. B* **113**, 9681–9686 (2009).

<sup>8</sup>X.-L. Zhang, X. Zhao, Z.-B. Liu, S. Shi, W.-Y. Zhou, J.-G. Tian, Y.-F. Xu, and Y.-S. Chen, "Nonlinear optical and optical limiting properties of graphene oxide-Fe<sub>3</sub>O<sub>4</sub> hybrid material," *J. Opt.* **13**, 075202 (2011).

<sup>9</sup>G.-K. Lim, Z.-L. Chen, J. Clark, R. G. S. Goh, W.-H. Ng, H.-W. Tan, R. H. Friend, P. K. H. Ho, and L.-L. Chua, "Giant broadband nonlinear optical absorption response in dispersed graphene single sheets," *Nat. Photonics* **5**, 554–560 (2011).

<sup>10</sup>M. B. M. Krishna, V. P. Kumar, N. Venkatramiah, R. Venkatesan, and D. N. Rao, "Nonlinear optical properties of covalently linked graphene-metal porphyrin composite materials," *Appl. Phys. Lett.* **98**, 081106 (2011).

<sup>11</sup>A. B. Bourlinos, A. Bakandritsos, N. Liaros, S. Couris, K. Safarova, M. Otyepka, and R. Zbořil, "Water dispersible functionalized graphene fluoride with significant nonlinear optical response," *Chem. Phys. Lett.* **543**, 101–105 (2012).

<sup>12</sup>N. Liaros, K. Iliopoulos, M. Stylianakis, E. Koudoumas, and S. Couris, "Optical limiting action of few layered graphene oxide dispersed in different solvents," *Opt. Mater.* **36**, 112–117 (2013).

<sup>13</sup>Y. Hernández, V. Nicolosi, M. Lotya, F. M. Blighe, Z. Sun, S. De, M. T. B. Holland, M. Byrne, Y. K. Gun'Ko, J. J. Boland, P. Niraj, G. Duesberg, S. Krishnamurthy, R. Goodhue, J. Hutchison, V. Scardaci, A. C. Ferrari, and J. N. Coleman, "High-yield production of graphene by liquid-phase exfoliation of graphite," *Nat. Nanotechnol.* **3**, 563–568 (2008).

<sup>14</sup>M. P. Lavin-López, J. L. Valverde, L. Sánchez-Silva, and A. Romero, "Solvent-based exfoliation via sonication of graphitic materials for graphene manufacture," *Ind. Eng. Chem. Res.* **55**, 845–855 (2016).

<sup>15</sup>Y. Feng, N. Dong, G. Wang, Y. Li, S. Zhang, K. Wang, L. Zhang, W. J. Blau, and J. Wang, "Saturable absorption behavior of free-standing graphene polymer composite films over broad wavelength and time ranges," *Opt. Express* **23**, 559–569 (2015).

<sup>16</sup>A. A. Murray and W. Blau, "Nonlinear properties of graphene dispersions and thin films at a wavelength of 1.2  $\mu\text{m}$ ," *J. Nanoelectron. Optoelectron.* **8**, 23–27 (2013).

<sup>17</sup>Y. Feng, N. Dong, Y. Li, X. Zhang, C. Chang, S. Zhang, and J. Wang, "Host matrix effect on the near infrared saturation performance of graphene absorbers," *Opt. Mater. Express* **5**, 802–808 (2015).

- <sup>18</sup>J. Wang, Y. Hernandez, M. Lotya, J. N. Coleman, and W. J. Blau, "Broadband nonlinear optical response of graphene dispersions," *Adv. Mater.* **21**, 2430–2435 (2009).
- <sup>19</sup>M. Miranda, C. L. Arnold, T. Fordell, F. Silva, B. Alonso, R. Weigand, A. L'Huillier, and H. Crespo, "Characterization of broadband few-cycle laser pulses with the d-scan technique," *Opt. Express* **20**, 18732–18743 (2012).
- <sup>20</sup>G. M. Morales, P. Schifani, G. Ellis, C. Ballesteros, G. Martinez, C. Barbero, and H. J. Salavagione, "High-quality few layer graphene produced by electrochemical intercalation and microwave-assisted expansion of graphite," *Carbon* **49**, 2809–2816 (2011).
- <sup>21</sup>U. Khan, A. O'Neill, M. Lotya, S. De, and J. N. Coleman, "High-concentration solvent exfoliation of graphene," *Small* **6**, 864–871 (2010).
- <sup>22</sup>A. C. Ferrari, "Raman spectroscopy of graphene and graphite: Disorder, electron phonon coupling, doping and nonadiabatic effects," *Solid State Commun.* **143**, 47–57 (2007).
- <sup>23</sup>L. G. Cançado, A. Jorio, E. H. M. Ferreira, F. Stavale, C. A. Achete, R. B. Capaz, M. V. O. Moutinho, A. Lombardo, T. S. Kulmala, and A. C. Ferrari, "Quantifying defects in graphene via raman spectroscopy at different excitation energies," *Nano Lett.* **11**, 3190–3196 (2011).
- <sup>24</sup>Z. Tu, Z. Liu, Y. Li, F. Yang, L. Zhang, Z. Zhao, C. Xu, S. Wu, H. Liu, H. Yang, and P. Richard, "Controllable growth of 1-7 layers of graphene by chemical vapour deposition," *Carbon* **73**, 252–258 (2014).
- <sup>25</sup>J. Wang, B. Gu, H.-T. Wang, and X.-W. Ni, "Z-scan analytical theory for material with saturable absorption and two-photon absorption," *Opt. Commun.* **283**, 3525–3528 (2010).
- <sup>26</sup>B. G. Yust, N. Razavi, F. Pedraza, Z. Elliott, A. T. Tsin, and D. K. Sardar, "Enhancement of nonlinear optical properties of batio3 nanoparticles by the addition of silver seeds," *Opt. Express* **20**, 26511–26520 (2012).
- <sup>27</sup>M. Falconieri, "Thermo-optical effects in z-scan measurements using high-repetition-rate lasers," *J. Opt. A* **1**, 662–667 (1999).
- <sup>28</sup>N. A. George, "Enhancement of nonlinear optical properties of BaTiO<sub>3</sub> nanoparticles by the addition of silver seeds: Comment," *Opt. Express* **25**, 18056–18057 (2017).
- <sup>29</sup>F. L. S. Cuppo, A. M. F. Neto, S. L. Gómez, and P. Palfy-Muhoray, "Thermal-lens model compared with the Sheik-Bahae formalism in interpreting z-scan experiments on lyotropic liquid crystals," *J. Opt. Soc. Am. B* **19**, 1342–1348 (2002).
- <sup>30</sup>M. Falconieri and G. Salvetti, "Simultaneous measurement of pure-optical and thermo-optical nonlinearities induced by high-repetition-rate, femtosecond laser pulses: Application to CS<sub>2</sub>," *Appl. Phys. B* **69**, 133–136 (1999).
- <sup>31</sup>S. M. Mian, S. B. McGee, and N. Melikechi, "Experimental and theoretical investigation of thermal lensing effects in mode-locked femtosecond z-scan experiments," *Opt. Commun.* **207**, 339–345 (2002).
- <sup>32</sup>M. González-Cardel, P. Arguijo, and R. Díaz-Urbe, "Gaussian beam radius measurement with a knife-edge: A polynomial approximation to the inverse error function," *Appl. Opt.* **52**, 3849–3855 (2013).